Nanoscale

Spray coating of the PCBM electron transport layer significantly improves the efficiency of p-i-n planar perovskite solar cells

Journal:	*Nanoscale*
Manuscript ID	NR-ART-03-2018-001763
Article Type:	Paper
Date Submitted by the Author:	01-Mar-2018
Complete List of Authors:	Zheng, Yifan; Yale University,Chemical and Enironmental Engineering, ; University of Electronic Science and Technology of China, optoelectronics information Kong, Jaemin; Yale University, Chemical and Environmental Engineering Di, Huang; Beijing Jiaotong University, Key Laboratory of Luminescence and Optical Information Ministry of Education, Beijing,; Yale University, Chemical and Environmental Engineering Shi, Wei; University of Electronic Science and Technology of China, McMillon-Brown, Lyndsey; Yale University Katz, Howard; Johns Hopkins University, Materials Science and Engineering Yu, Junsheng; University of Electronic Science and Technology of China, Taylor, Andre; Yale University, Chemical and Environmental Engineering

Nanoscale

Paper

Spray coating of the PCBM electron transport layer significantly improves the efficiency of p-i-n planar perovskite solar cells†

Received 00th January 20xx,
Accepted 00th January 20xx

DOI: 10.1039/x0xx00000x

www.rsc.org/

Yifan Zheng[ab], Jaemin Kong[b], Di Huang[b], Wei Shi[ac], Lyndsey McMillon-Brown[b], Howard E. Katz[c], Junsheng Yu[a]* and André D. Taylor[b]*

The p-i-n structure for perovskite solar cells has recently shown significant advantages in minimal hysteresis effects, and scalable manufacturing potential using low-temperature solution processing. However, the power conversion efficiency (PCE) of the perovskite p-i-n structure remains low mainly due to limitations using a flat electron transport layer (ETL). In this work, we demonstrate a new approach using spray coating to fabricate the [6,6]-phenyl-C(61)-butyric acid methyl ester (PCBM) ETL. By creating a rough surface, we effectively improve the light trapping properties inside the PCBM ETL. We reveal that the spray coated PCBM can form a cross-linked network which may facilitate better charge transport and enhance extraction efficiency. By improving the contact between the perovskite film and the PCBM ETL, a reduction in the trap states is observed resulting in a PCE increase from 13% to > 17%.

Introduction

Hybrid inorganic-organic perovskite solar cells as the next generation solar cells, have rapidly increased in power conversion efficiency (PCE) from 3% to over 22%.[1-5] As a result, the study of perovskite solar cells have garnered a strong research focus that was once traditionally directed at Si, CIGS, CdTe and polymer solar cells.[4, 6, 7] Organic halide perovskites have ABX_3 crystal structures, where A, B, and X are organic cations, metal cation and halide anion, respectively.[8-11] Up to now, a variety of perovskites have been explored, including $CH_3NH_3PbX_3$ (X=I, Cl, Br), $CH(NH_2)_2PbI_3$, $CH_3NH_3SnI_3$ and their solid solutions.[7, 12, 13] However, only the mesoporous and planar device architectures have been mainly studied in perovskite solar cells,[14-17] Although the early successful perovskite solar cells were first demonstrated as a mesoporous device, the high sintering temperature of the titanium dioxide that forms a heterojunction with the perovskite and the deleterious J-V hysteresis dramatically affected the fabrication efficiency and working stability of these devices.[18, 19] In contrast, due to the long diffusion length over 175 nm and ambipolar behaviour of perovskite, the PCE of planar perovskite solar cells significantly improved from 4% in 2013 to recently over 20%, which is comparable to the mesoporous perovskite solar cell architecture.[3, 20]

In general, a planar structure can be divided categorically into either a regular planar (p-i-n) or an inverted planar (n-i-p) type.[20, 21] P-i-n planar perovskite solar cells present several advantages such as minor hysteresis effects, low-temperature solution processibility, and the potential for large-scale manufacturing using a continuous deposition technique on flexible substrates.[19, 21-27] In addition to the quality of the perovskite layer, the hole transport layer (HTL; adjacent to the bottom, hole-extracting electrode) and the electron transport layer (ETL; just below the top, electron-extracting electrode) are critical to the device performance. Previously, several efficient HTLs have been investigated that favour the formation of crystalline perovskite.[25, 28-31] However, the situation is quite different for the ETL in the planar p-i-n design. In this case, the ETL solution is deposited on top of the perovskite film and should therefore cover the entire perovskite surface without dissolving the underlying perovskite layer.[32] When compared to the diversity of available HTLs, the selection of the ETL is quite limited. Fullerenes, especially [6,6]-phenyl-C(61)-butyric acid methyl ester (PCBM), are the most efficient n-type charge transport layer and have been shown to work well in the planar p-i-n perovskite solar cells.[32-36]

However, there are several limitations with regard to the conventional fabrication of the flat PCBM ETL for the planar p-i-n perovskite solar cell. Firstly, the surface morphology of the spin cast flat PCBM ETL is largely dependent on the underlying perovskite morphology.[37] For instance, the large spacing between the perovskite grains can leave openings or very thin regions in the surface of the ETL. During the electrode deposition, hot metal atoms could have the potential to permeate through these openings to form a direct contact with the perovskite active layer,

[a] State Key Laboratory of Electronic Thin Films and Integrated Devices, School of Optoelectronic Information, University of Electronic Science and Technology of China (UESTC), Chengdu 610054, P. R. China. E-mail: jsyu@uestc.edu.cn.
[b] Y. Zheng, Dr. J. Kong, D. Huang, L. McMillon-Brown, Prof. A. Taylor, Department of Chemical and Environmental Engineering, Yale University, New Haven, Connecticut, 06511, United States. E-mail: andre.taylor@yale.edu, yifan.zheng@yale.edu.
[c] Department of Materials Science and Engineering, Johns Hopkins University, 3400 North Charles Street, Baltimore, Maryland, 21218, United States. E-mail: hekatz@jhu.edu
†. Electronic Supplementary Information (ESI) available. See DOI: 10.1039/x0xx00000x

resulting in the quenching of excitons.[38-40] Secondly, a high concentration of the PCBM solution is necessary in order to make sure the ETL fully covers the perovskite film by spin coating. However, almost 80% of the solution can be wasted during spin coating, leading to a higher cost for scalable fabrication.[41, 42] Thirdly, devices based on spin cast thin films suffer from a restricted current density, which is attributed to the imbalance between the light absorption efficiency and the film thickness.[23, 37, 43] Many attempts have been made to further improve the performance of perovskite solar cells via modifying the PCBM ETL. The fullerene derivatives, including [6, 6]-phenyl C(71)-butyric acid methyl ester ($PC_{70}BM$), indene-C60 bisadduct (ICBA) and C_{60}, are typically combined with PCBM to achieve an improved energy level match and charge transport efficiency.[2, 43, 44] For example, some metal oxides such as zinc oxide and titanium dioxide have been associated with PCBM to afford a better ohmic contact and device stability.[45] Furthermore, small molecule materials including rhodamine 101 zwitterion and perylene-diimide have also been introduced in the PCBM ETL system to provide a higher quality contact with the top Ag electrode.[16, 46] Unfortunately, these modifications still result in relatively low PCEs due to the unsolved perovskite/PCBM interface problems. We note that the addition of C_{60} to spin cast PCBM by thermal evaporation can produce a high efficiency control device, but also adds an additional expensive material and processing step.[3, 24, 47]

We suggest that the use of a rough single layer PCBM ETL offers the possibility of an improved ohmic contact with a less penetrable interface contact and enhanced light trapping.[24, 35, 48] Although several kinds of rough film techniques have been introduced into organic solar cells, the successful application of them in perovskite solar cells has not yet been fully realized.[49-51] Hence, knowledge of how to attain a rough PCBM ETL using a concise and low cost method to improve the PCE baseline can contribute to the development of perovskite solar cells with enhanced performance. In this work, we show that spray coating can be an effective approach for depositing the PCBM ETL for planar p-i-n perovskite solar cells. Compared with the general spin coating approach, the spray coated PCBM ETL device exhibits an extremely high short circuit current density (J_{SC}) of 22.4 mA/cm^2 and open circuit voltage (V_{OC}) of 1.05 V. Through characterizing the surface morphology by atomic force microscopy (AFM), together with diffusion reflection detection, we reveal that the rough PCBM film has a low defect density compared to other ETLs and efficiently reflects the incident light back to the perovskite film for reabsorption. These modifications result in a 30% enhancement in the PCE, from 13% to 17%.

Results and Discussion

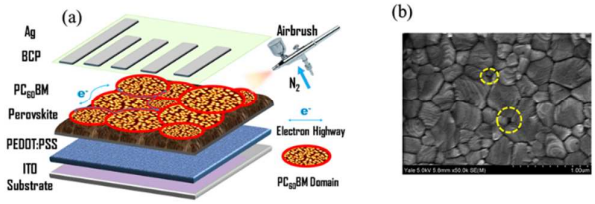

Figure 1 (a) Schematic image of a regular planar p-i-n device architecture. (b) SEM image of the surface of perovskite film. The pin-holes have been marked by yellow circles.

The device architecture used in this work is shown in **Figure 1a**. We characterize the surface of the $CH_3NH_3IPbI_3$ film by using scanning electron microscope (SEM). We show that the crystalline domain size of the perovskite ranges from 100 nm to 400 nm (**Figure 1b**). It is found that the grain size is not homogeneous, leading to pin-holes existing on the edges of grains (marked by yellow circles). When we spin cast a PCBM layer on the top of this perovskite film, we notice using an optical microscope significant PCBM aggregation centers with a size of about 10 μm (**Figure S1a**). We illustrate this inhomogeneous distribution of PCBM molecules as blue regions that relate to thicker PCBM film areas whereas the yellow parts represent the thinner areas. Conversely, our spray coating technique deposits a homogenous film without showing any aggregation centers (**Figure S1b**). The spray coating by using our airbrush technique combines gas and solution together as an aerosol spray.[41, 52] Through the precise control of the spray coating parameters that include spray rate, gas pressure, and the solution concentration, we can optimize the film morphology by modifying the quality of the atomized droplets, viscosity of solution and impact velocity of the droplets hitting the substrate.[53-55] Upon optimization of these parameters, we observe an array of uniform droplets that appear to be a closely packed PCBM particle mat (**Figure S1b**).[42, 56] In addition, a network of coffee-ring-effect aggregates forms over this mat.

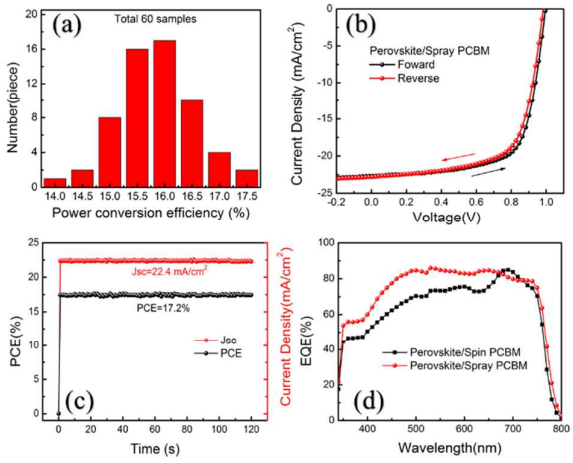

Figure 2 (a) Histogram of average efficiency for 60 devices. (b) J-V curves for best cell measured by forward and reverse scans. (c) EQE curves of the perovskite solar cells based on spin and spray PCBM ETL. (d) Steady-state measurement of J_{SC} and PCE for PSC based on 100 nm spray coated PCBM.

It is well known that the thickness of the PCBM ETL is critical to the device performance.[35, 36] In order to make a fair comparison between the spray and the spin coated PCBM, we can adjust the thickness of the spray PCBM ETL by simply varying the PCBM solution concentration. We show a summary of spin coated PCBM ETL devices (**Figure S2**) and detail the parameters in **Table 1**. The best ETL thickness for our cells is in the range of 55 ± 5 nm, which gives an average PCE of 13.56%. We note that at thicknesses above

and below this value, the devices suffer from a lower short circuit current density (J_{SC}) and fill factor (FF).[36] Compared with spin coated ETL, the spray coated films will have a rougher surface and a higher thickness.[41, 53] In this case, we vary the thickness from 60 nm to 120 nm every 20 nm (**Figure S3**). We observe that the spray coated device J_{SC} is higher (ca. 22.5 mA/cm^2) than the control cells (ca. 18 mA/cm^2), and independent of the PCBM thickness. This trend is also found in the V_{OC} where the spray coated devices exhibit a relatively high V_{OC} (>1 V) compared to the control cells (ca. 0.85 V). However, we notice that the spray coated device FF is dependent on the ETL thickness. For a 60 nm PCBM ETL, the FF is only 65% in comparison to the optimized spin cast device FF of ca. 80%. We speculate that this result may be from the uneven contact between the PCBM and the silver electrode due to the rougher surface.[42] In this case, the penetration of hot silver molecules from the top electrode through the ETL and into the perovskite film could more readily happen with a rough surface thin film causing a large leakage current and low FF.[41, 42] By increasing the ETL thickness, the FF steadily rises to 73%. When the thickness is further increased above 120 nm, the FF decreases because of the inefficient extraction of electrons.[3, 7] Through optimizing the spray parameters and PCBM ETL thickness, we demonstrate perovskite solar cells with a V_{OC} of 1.05 V, a J_{SC} of 22.4 mA/cm^2, a FF of 73.2%, and a PCE of 17.26 %. More importantly, good reproducibility is also demonstrated (**Figure 2a**). Over 60 % of the devices based on the spray coated PCBM ETL achieve a significant PCE enhancement from 13 % to more than 16 % compared to the average of optimized spin-coated devices.

Table 1 Summary of device parameters.

ETL[a]	Thickness(nm)	V_{OC}[b](V)	J_{SC}[b](mA/cm^2)	FF[b](%)	PCE[b](%)
Spin PCBM	45±5	0.90±0.1	17.6±0.2	78.6±0.3	12.49±0.2
	55±5	0.89±0.1	19.0±0.3	79.9±0.2	13.56±0.2
	65±5	0.90±0.1	16.7±0.3	78.4±0.3	11.70±0.3
Spray PCBM	60±10	1.04±0.1	22.6±0.1	65.5±0.5	15.48±0.2
	80±20	1.03±0.1	22.7±0.2	73.2±0.4	16.62±0.3
	100±20	1.05±0.1	22.4±0.3	73.2±0.4	17.26±0.3
	120±20	0.99±0.2	22.7±0.2	69.4±0.3	15.68±0.2

[a] The device structure is ITO/PEDOT:PSS/$CH_3NH_3PbI_3$/PCBM/BCP/Ag.

[b] All the numbers listed in the table are the average values from 15 devices.

By measuring the devices with forward and reverse scanning, the control, spin coated PCBM cell presents an obvious J-V hysteresis, which is attributed to the dynamic electric field/charge injection modulated charge trapping and detrapping.[18, 19, 24] Although the PCBM film can effectively passivate the charge traps in the perovskite films, the high aggregation of PCBM could create new charge trap centers (**Figure S1a**).[21] This photocurrent hysteresis imposes a serious issue on the accurate determination of the efficiency and stability of perovskite solar cells (**Figure S4**).[23, 24] In contrast, only minor hysteresis is observed in the spray coated PCBM ETL device (**Figure 2b**). This result indicates that the spray coated PCBM with homogeneous distribution of interconnected PCBM particles can significantly passivate the charge traps in both the perovskite film and the PCBM ETL. In addition, the PSCs based on spray coated PCBM ETL exhibit low photocurrent hysteresis, indicating that the spray coated PCBM can efficiently block the ion-migration channel at the grain boundaries (**Figure 2c**). Moreover, the uniform PCBM layer provides an efficient channel for charge transfer. A faster charge transfer between the perovskite film and the PCBM ETL is consistent with a decreased capacitance associated with charge that inhibits charge extraction, resulting in a relatively high J_{SC}.[32, 35] We found that this J_{SC} can be verified by the higher EQE of the spray coated PCBM device across almost the entire wavelength range from 350 nm to 700 nm (**Figure 2d**). We also notice that the EQE peaks around 400 nm to 500 nm increase significantly compared with the EQE peak at around 700 nm. The improvement in the EQE may be ascribed to the more efficient charge transport in the perovskite/ETL interface, and the increased light absorption inside the perovskite film.[37, 48] We speculate that the high roughness of the spray coated PCBM film surface will reflect more light back to the perovskite film for reabsorption.

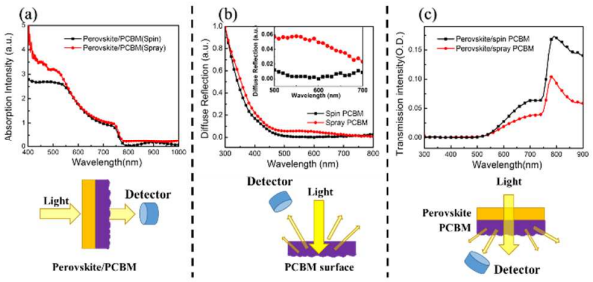

Figure 3 (a) The absorption of perovskite/PCBM thin film. (b) Diffuse reflection spectra of spin and spray coated PCBM film. Insert: Diffuse reflection spectra of the PCBM film between 500 to 700 nm (c) Diffuse transmission of perovskite/PCBM film. Bottom images present the absorption, diffuse reflection, and diffuse transmission test equipment used in this work, respectively.

To verify our hypothesis, we investigate the optical properties of the device by first looking at the absorption of the spin and spray perovskite/PCBM layers. We illustrate that the spray coated PCBM shows a much higher absorption between 400-550 nm which contributes to increasing the J_{SC} (**Figure 3a**). Between 600-800 nm, the absorption intensity of the spray coated device is slightly higher than the spin coated one. Next, we evaluate the diffuse reflection of the spin and spray PCBM ETLs (**Figure 3b**). We show that the spin coated PCBM ETL has a lower diffuse reflection intensity in the whole wavelength range from 300 nm to 800 nm, especially between 450 nm to 700 nm. The absorption peak of the PCBM is located at ca. 400 nm, which means the incident light with lower energy can transmit through the PCBM film or be diffuse-reflected back.[57] We associate this higher diffuse reflection intensity with a higher possibility for the perovskite film to reabsorb light (**Figure 3b**). Furthermore, we test the diffuse transmission properties of the perovskite/PCBM ETL. The spin coated PCBM allows more light to pass through it due to the relatively smooth surface. In comparison, the spray coated PCBM exhibits lower diffusion transmission intensity in the wavelength range between 500 to 700 nm, which is attributed to the rough surface of the PCBM. These results indicate that more incident light from 500 to 700 nm is diffusely reflected back to the perovskite film for reabsorption, and this is also consistent with the results of the diffusion reflection test.

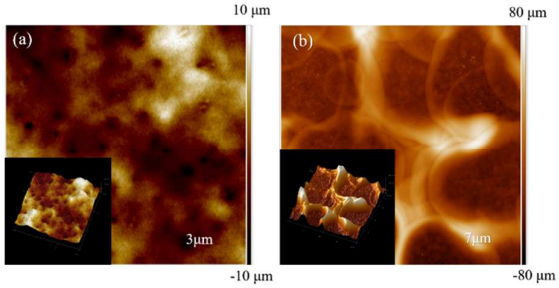

Figure 4 AFM height image of (a) spin coated PCBM and (b) spray coated PCBM ETL on the top of perovskite, inset: the 3D image of the film morphology correspondingly.

To gain more insight into the effect of the spray coated PCBM ETL on the device performance, we characterize in detail the morphology of the PCBM ETL by AFM. It is well known that solution processed PCBM films have a strong tendency towards forming aggregates during the film drying process.[58] We show that there are several isolated peaks on the surface of the spin cast flat PCBM film with a height of about 10 nm (**Figure S5a** and **c**). These peaks are formed by PCBM aggregation, resulting in the root mean square (RMS) roughness of 5.2 nm. For comparison, the spray coated PCBM extends to a height of over 60 nm (**Figure S5b** and **d**), leading to high RMS of 35 nm. When we fabricate the PCBM on the top of the perovskite film, the processing of the spin and spray PCBM are very different. Several openings with a size of about 120 nm could be observed in the surface of perovskite/PCBM (spin) film, which results from the aggregation of the PCBM and the rough perovskite surface (**Figure 4a**, **Figure S6a** and **c**). These openings may function as trap centres that decrease the electron transfer efficiency.[2, 23, 44] In contrast, most of these openings disappear when we spray PCBM ETL, which may attribute to a much more complete contact between the perovskite and the ETL. A high pressure of nitrogen gas increases the impact of the PCBM droplet to the perovskite surface (**Figure 4b**, **Figure S6b** and **d**). Without these openings, a more efficient charge extraction in the perovskite/PCBM interface will make a contribution to a higher V_{OC} and J_{SC}. It is interesting to find that the J_{SC} is independent of the thickness of the spray coated PCBM. This indicates that the electrons may have higher mobility in these interconnected networks (**Figure S7a** and **b**). Although the surface of the spray coated PCBM ETL is comparatively rough (~ 60 nm), it does not seem to decrease the charge transport efficiency, which is verified by the electron mobility test in organic thin film transistors (**Figure S8**).[34] The electron mobility of this fairly isotropic PCBM film increases from 1.5×10^{-3} cm^2/Vs (for spin coated) to 3.3×10^{-3} cm^2/Vs for spray coated PCBM.[34, 52]

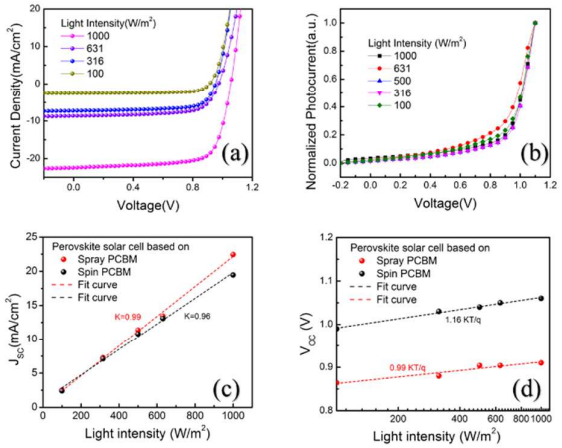

Figure 5 (a) light intensity dependence *J-V* curve of devices. (b) Normalized light intensity depended *J-V* curve. (c) J_{SC} plotted against incident light intensity for the device based on spin or spray coated PCBM ETL. (d) Logarithmic dependence of V_{OC} with incident light intensity.

To investigate the recombination mechanism, we measure the light intensity dependent current-voltage characteristics of the perovskite solar cells (**Figure 5a**). The data from all curves shown in **Figure 5a** collapse onto a universal voltage dependence in the range of applied voltages from -0.2 V to 0.7 V, indicating the carrier sweep-out is not generation-rate dependent and that recombination is minimal.[37, 59] The results of normalized light intensity dependent current-voltage characteristics represent the monomolecular and bimolecular domination areas, which are located in the ranges of -0.2 V to 0.5 V and 0.8 V to 1.2 V, respectively (**Figure 5b**). We illustrate the power law dependence of the J_{SC} with light intensity ($J\propto I^{\alpha}$) where I is the light intensity and α is the exponential factor (**Figure 5c**). An α value close to unity indicates weak bimolecular recombination,[59, 60] whereas an exponent α less than 1 could result from bimolecular recombination, space charge effects, variation in mobility between the two carriers or variation in the continuous distribution in the density of states. We calculate that the spray coated PCBM ETL device has an α of 0.99 while the device of spin coated PCBM ETL shows an α of 0.96. The large aggregation of PCBM and the defect centres displayed as pores are expected to accumulate charges and form potential barriers. In this case, charge extraction is limited in the spin coated PCBM devices. The slope of the V_{OC} versus the natural logarithm of the light intensity implies that bimolecular recombination is the dominant mechanism limiting the open circuit, where k, T, q are the Boltzmann constant, temperature in Kelvin, and the elementary charge, respectively.[59] The slopes for the device with spin and spray PCBM ETL are 1.16 kT/q and 0.99 kT/q, respectively (**Figure 5d**). The stronger dependence of V_{OC} on light intensity implies that recombination at open circuit in this device is a combination of monomolecular (SRH) and bimolecular process.[37, 59] The lower slope of the spray coated PCBM device indicates this ETL reduces the density of interfacial traps between the perovskite and electrode contact, and hence SRH recombination is restricted.[60]

Conclusions

In summary, we demonstrate a significant enhancement in p-i-n perovskite solar cell PCEs from 13% to over 17% by incorporating a spray coated PCBM ETL. Through characterizing the surface morphology and optical parameter of spray coated PCBM ETL, we find that the rough surface can effectively improve the light trapping inside the PCBM ETL. Moreover, the interconnected network of the PCBM improves the electron extraction efficiency and prevents charge accumulation at the interface. We show that a spray coated PCBM ETL layer forms an improved contact between the perovskite film and the PCBM ETL which results in the reduction of trap states for a higher V_{OC}. We also demonstrate that this approach is highly reproducible, concise and practical for perovskite solar cells, paving a promising way for the further achievement of scalable high performance perovskite solar cells.

Experimental section

***Materials and reagents*:** All solvents and reagents are analytically pure quality and used as received. Poly (3,4-ethylenedioxythiophene)-polystyrenesulfonic acid (PEDOT:PSS) (99%, Heraeus), lead iodide (PbI_2) (99% Alfa Aesar), methylammonium iodide (CH_3NH_3I) (98% Sigma-Aldrich), PCBM (99 % 1-Material), molybdenum trioxide (99% American Elements), 2,9-dimethyl-4,7-diphenyl-1,10-phenanthroline (BCP) (99% Lumitech), silver (Ag) (99% International Advanced Materials), chlorobenzene (CB) (99.8% Sigma-Aldrich), dimethyl formamide (DMF) (99% Sigma-Aldrich).

Fabrication of perovskite solar cell: In this work, we use the p-i-n architecture of ITO/ PEDOT:PSS/ $CH_3NH_3PbI_3$/ PCBM/ BCP/ Ag (**Figure 1a**). ITO-coated glass substrates with a sheet resistance of 10 Ω/sq were consecutively cleaned in ultrasonic bath containing detergent, acetone, deionized water and ethanol for 10 min each step, then dried by nitrogen. Prior to film deposition, the substrate was treated by UV light for 15 min. For PEDOT:PSS film fabrication, we spin coated PEDOT:PSS with a spin rate of 4000 rpm, 20s, followed by thermal annealing in 150 ^{o}C for 15 min. CH_3NH_3I and PbI_2 were mix together in DMF with a mole ratio of 1:1 for overnight. Perovskite film was spin coated with a rate 6000 rpm 25s inside the N_2 glove box, using chlorobenzene to wash the surface as described by N.J. Jeon et al.[5] After waiting for 5 min, the perovskite film was placed on a hot plate for thermal annealing in 100 ^{o}C for 5 min. For the control cell, 30 mg/ml PCBM was spun in a rate of 2000 rpm 20s inside the glove box. For spray coating, samples were placed in the ambient air. PCBM solution with a concentration of 5 mg/ml were spray coated onto the perovskite film at a height of 10 cm, a gas pressure of 70 psi, and a spray rate of 2.5 µl/s. The devices were finally realized by evaporating 2 nm BCP and 100 nm Ag in the metal deposition chamber under the vacuum ≤ 10^{-6} torr.

Characterization of perovskite solar cells: After fabrication, devices were illuminated at 100 mW/cm^2 from a 150 W solar simulator with AM 1.5G filters (PV Measurements). The illumination intensity was determined by a National Renewable Energy Laboratory (NREL) calibrated Si solar cell with KG-5 color filter. All electrical measurements were carried out in air at room temperature. The active area of the device irradiated by the light was defined as 1.8 cm^2 using a photomask, so no extra current outside of the defined area was collected. Current density-voltage (*J-V*) curves were measured with a Keithley 2400 source measurement unit. The external quantum efficiency (EQE) measurements were performed using a PV Measurements QEX7 system. All the measurements mentioned above were taken inside the N_2 glove box. The morphology of active layer was characterized by AFM (MFP-3D-BIO, Asylum Research). The perovskite solar cell absorption, spectra were measured by a UV-Vis spectrometer (LAMBDA 950, PerkinElmer). The diffuse reflection and transmission spectra were measured using a commercial integrating sphere setup (LabSphere).

Acknowledgements

This research was funded by the Foundation of the National Natural Science Foundation of China (NSFC) (Grant No. 61675041), and the Foundation for Innovation Research Groups of the NSFC (Grant No. 61421002). The authors gratefully acknowledge the Chinese Scholarship Council (No. 201506070069) and National Science Foundation NSF-PECASE award (CBET-0954985), for partial support of this work. The Yale Institute for Nanoscience and Quantum Engineering (YINQE) and NSF MRSEC DMR 1119826 (CRISP) provided facility support. The author also thanks Prof. B. Rand and Dr. Y. Lin for providing the diffuse reflection and transmission measurement.

Notes and references

1. C. V. Hoven, A. Garcia, G. C. Bazan and T. Q. Nguyen, *Adv. Mater.*, 2008, **20**, 3793-3810.
2. Y. Xing, C. Sun, H. L. Yip, G. C. Bazan, F. Huang and Y. Cao, *Nano Energy*, 2016, **26**, 7-15.
3. Q. Wang, Q. Dong, T. Li, A. Gruverman and J. Huang, *Adv. Mater.*, 2016.
4. M. A. Green, A. Ho-Baillie and H. J. Snaith, *Nature Photonics*, 2014, **8**, 506-514.
5. N. J. Jeon, J. H. Noh, Y. C. Kim, W. S. Yang, S. Ryu and S. I. Seok, *Nat. Mater.*, 2014, **13**, 897-903.
6. J. Min, Z.-G. Zhang, Y. Hou, C. O. R. Quiroz, T. Przybilla, C. Bronnbauer, F. Guo, K. Forberich, H. Azimi, T. Ameri, E. Spiecker, Y. Li and C. J. Brabec, *Chem. Mater.*, 2015, **27**, 227-234.
7. C.-C. Chueh, C.-Z. Li and A. K. Y. Jen, *Energy Environ. Sci.*, 2015, **8**, 1160-1189.
8. D. B. Mitzi, *Inorg. Chem.*, 2000, **39**, 6107-6113.
9. K. D. Karlin, *Progress in inorganic chemistry*, John Wiley & Sons, 2011.
10. D. B. Mitzi, C. D. Dimitrakopoulos and L. L. Kosbar, *Chem. Mater.*, 2001, **13**, 3728-3740.
11. D. B. Mitzi, *J. Chem. Soc.*, 2001, 1-12.
12. J. W. Lee, D. J. Seol, A. N. Cho and N. G. Park, *Adv. Mater.*, 2014, **26**, 4991-4998.
13. P. Umari, E. Mosconi and F. De Angelis, *Sci. Rep.*, 2014, **4**.
14. M. M. Lee, J. Teuscher, T. Miyasaka, T. N. Murakami and H. J. Snaith, *Science*, 2012, **338**, 643-647.

15. J. H. Heo, D. H. Song, H. J. Han, S. Y. Kim, J. H. Kim, D. Kim, H. W. Shin, T. K. Ahn, C. Wolf, T.-W. Lee and S. H. Im, *Adv. Mater.*, 2015, **27**, 3424-3430.
16. K. Sun, J. Chang, F. H. Isikgor, P. Li and J. Ouyang, *Nanoscale*, 2015, **7**, 896-900.
17. H. Wu, C. J. Zhang, K. X. Ding, L. J. Wang, Y. L. Gao and J. L. Yang, *Org. Electron.*, 2017, **45**, 302-307.
18. H. J. Snaith, A. Abate, J. M. Ball, G. E. Eperon, T. Leijtens, N. K. Noel, S. D. Stranks, J. T.-W. Wang, K. Wojciechowski and W. Zhang, *J. Phys. Chem. Lett.*, 2014, **5**, 1511-1515.
19. H. Zhou, Q. Chen, G. Li, S. Luo, T.-b. Song, H.-S. Duan, Z. Hong, J. You, Y. Liu and Y. Yang, *Science*, 2014, **345**, 542-546.
20. N. J. Jeon, J. H. Noh, Y. C. Kim, W. S. Yang, S. Ryu and S. I. Seok, *Nature materials*, 2014, **13**, 897-903.
21. J. Y. Jeng, Y. F. Chiang, M. H. Lee, S. R. Peng, T. F. Guo, P. Chen and T. C. Wen, *Adv. Mater.*, 2013, **25**, 3727-3732.
22. J. Liu, S. Chen, D. Qian, B. Gautam, G. Yang, J. Zhao, J. Bergqvist, F. Zhang, W. Ma, H. Ade, O. Inganäs, K. Gundogdu, F. Gao and H. Yan, *Nat. Energy*, 2016, **1**, 16089.
23. H. Kim, K. G. Lim and T. W. Lee, *Energy Environ. Sci.*, 2016, **9**, 12-30.
24. Y. Shao, Z. Xiao, C. Bi, Y. Yuan and J. Huang, *Nat. Comm.*, 2014, **5**, 5784.
25. D. Huang, T. Goh, J. Kong, Y. Zheng, S. Zhao, Z. Xu and A. D. Taylor, *Nanoscale*, 2017, **9**, 4236-4243.
26. Q. Hu, H. Wu, J. Sun, D. Yan, Y. Gao and J. Yang, *Nanoscale*, 2016, **8**, 5350-5357.
27. H. Yu, X. D. Liu, Y. J. Xia, Q. Q. Dong, K. C. Zhang, Z. W. Wang, Y. Zhou, B. Song and Y. F. Li, *J. Mater. Chem. A*, 2016, **4**, 321-326.
28. K. Domanski, W. Tress, T. Moehl, M. Saliba, M. K. Nazeeruddin and M. Grätzel, *Adv. Funct. Mater.*, 2015, **25**, 6936-6947.
29. M. Zhang, M. Lyu, H. Yu, J. H. Yun, Q. Wang and L. Wang, *Chemistry*, 2015, **21**, 434-439.
30. C. V. Kumar, G. Sfyri, D. Raptis, E. Stathatos and P. Lianos, *Rsc Adv.*, 2015, **5**, 3786-3791.
31. P. Nagarjuna, K. Narayanaswamy, T. Swetha, G. H. Rao, S. P. Singh and G. D. Sharma, *Electrochimica Acta*, 2015, **151**, 21-26.
32. X. Liu, H. Yu, L. Yan, Q. Dong, Q. Wan, Y. Zhou, B. Song and Y. Li, *Acs Appl. Mater. Inter.*, 2015, **7**, 6230-6237.
33. Y. Xing, C. Sun, H. Yip, G. C. Bazan, F. Huang and Y. Cao, *Nano Energy*, 2016, DOI: 10.1016/j.nanoen.2016.04.057, 7-15.
34. S. Nam, J. Jang, H. Cha, J. Hwang, T. K. An, S. Park and C. E. Park, *J. Mater. Chem.*, 2012, **22**, 5543-5549.
35. C.-H. Chiang and C.-G. Wu, *Nat. Photo.*, 2016, **10**, 196-200.
36. J. Seo, S. Park, Y. C. Kim, N. J. Jeon and J. H. Noh, *Energy Environ. Sci.*, 2014, **7**, 2642-2646.
37. N. Marinova, W. Tress, R. Humphry-Baker and M. I. Dar, *ACS nano*, 2015, **9**, 4200-4209.
38. S. T. Lee, Z. Q. Gao and L. S. Hung, *Appl. Phys. Lett.*, 1999, **75**, 1404-1406.
39. J. Wagner, M. Gruber, A. Wilke and Y. Tanaka, *J. Appl. Phys.*, 2012, **111**, 054509.
40. J. Meiss, M. K. Riede and K. Leo, *Appl. Phys. Lett.*, 2009, **94**, 013303.
41. Y. Zheng, R. Wu, W. Shi, Z. Guan and J. Yu, *Sol. Energy Mat. Sol. C.*, 2013, **111**, 200-205.
42. C. Girotto, D. Moia and B. P. Rand, *Adv. Funct. Mater.*, 2011, **21**, 64-72.
43. S. Shao, M. Abdu-Aguye, L. Qiu, L.-H. Lai, J. Liu, S. Adjokatse, F. Jahani, M. E. Kamminga, G. H. ten Brink, T. T. M. Palstra, B. J. Kooi, J. C. Hummelen and M. Antonietta Loi, *Energy Environ. Sci.*, 2016, **9**, 2444-2452.
44. P. W. Liang, C. C. Chueh and S. T. Williams, *Adv. Energy Mater.*, 2015, **5**, 1402321.
45. C. Huang, W. Fu, C. Z. Li, Z. Zhang, W. Qiu, M. Shi, P. Heremans, A. K. Jen and H. Chen, *J Am Chem Soc*, 2016, **138**, 2528-2531.
46. F. Fernández-Lázaro, N. Zink-Lorre and Á. Sastre-Santos, *J. Mater. Chem. A*, 2016, **4**, 9336-9346.
47. D. Zhao, M. Sexton, H.-Y. Park, G. Baure, J. C. Nino and F. So, *Adv. Energy Mater.*, 2015, **5**.
48. J. Shi, X. Xu, D. Li and Q. Meng, *Small*, 2015, **11**, 2472-2486.
49. J. Kim, P. Kim, N. C. Pégard, S. Oh, C. R. Kagan, J. W. Fleischer, H. A. Stone and Y.-L. Loo, *Nat. Photo.*, 2012, **6**, 327-332.
50. K. S. Nalwa, J.-M. M. Park, K.-M. M. Ho and S. Chaudhary, *Adv. Mater.*, 2011, **23**, 112-116.
51. S. Benagli, D. Borrello and E. Vallat-Sauvain, *Proceedings of the 24th European Photovoltaic Solar Energy Conference*, 2009, 2293-2298.
52. W. Shi, J. Yu, W. Huang and Y. Zheng, *J. Phys. D. Appl. Phys.*, 2014, **47**, 205402.
53. Y. Zheng, S. Li, X. Yu, D. Zheng and J. Yu, *Rsc Adv.*, 2014, **4**, 16464-16471.
54. F. S. Gittleson, D. J. Kohn, X. Li and A. D. Taylor, *ACS nano*, 2012, **6**, 3703-3711.
55. F. S. Gittleson, D. Hwang, W.-H. Ryu, S. M. Hashmi, J. Hwang, T. Goh and A. D. Taylor, *ACS nano*, 2015, **9**, 10005-10017.
56. R. D. Deegan, O. Bakajin, T. F. Dupont, G. Huber, S. R. Nagel and T. A. Witten, *Nature*, 1997, **389**, 827-829.
57. Y. H. Seo, J. S. Yeo, N. Myoung, S. Y. Yim, M. Kang, D. Y. Kim and S. I. Na, *ACS Appl. Mater. Inter.*, 2016, **8**, 12822-12829.
58. Y.-C. Huang, Y.-C. Liao, S.-S. Li, M.-C. Wu, C.-W. Chen and W.-F. Su, *Sol. Energy Mat. Sol. C.*, 2009, **93**, 888-892.
59. S. R. Cowan, A. Roy and A. J. Heeger, *Phys. Rev. B*, 2010, **82**, 245207.
60. V. Gupta, W. L. Leong, L. Ke, G. C. Bazan and A. J. Heeger, *ACS nano*, 2013, **7**, 4569-4577.